Original Paper

Comparing different segments in shut-in pressure signals: New insights into frequency range and energy distribution

Ya-Jing Wang [a, b], Xiao-Dong Hu [a, b, *], Fu-Jian Zhou [a, b], Pu-Kang Yi [a, b], Wei-Peng Guan [a, b], Yang Qiu [c], En-Jia Dong [a, b], Peng-Tian Zhang [a, b]

[a] State Key Laboratory of Oil and Gas Resources and Engineering, Beijing, 102249, China
[b] China University of Petroleum (Beijing), Beijing, 102249, China
[c] Beijing Research Institute of Chemical Engineering and Metallurgy, CNNC, Beijing, 101149, China

ARTICLE INFO

ABSTRACT

Water hammer diagnostics is an important fracturing diagnosis technique to evaluate fracture locations and other downhole events in fracturing. The evaluation results are obtained by analyzing shut-in water hammer pressure signal. The field-sampled water hammer signal is often disturbed by noise interference. Noise interference exists in various pumping stages during water hammer diagnostics, with significantly different frequency range and energy distribution. Clarifying the differences in frequency range and energy distribution between effective water hammer signals and noise is the basis of setting specific filtering parameters, including filtering frequency range and energy thresholds. Filtering specifically could separate the effective signal and noise, which is the key to ensuring the accuracy of water hammer diagnosis. As an emerging technique, there is a lack of research on the frequency range and energy distribution of effective signals in water hammer diagnostics. In this paper, the frequency range and energy distribution characteristics of field-sampled water hammer signals were clarified quantitatively and qualitatively for the first time by a newly proposed comprehensive water hammer segmentation-energy analysis method. The water hammer signals were preprocessed and divided into three segments, including pre-shut-in, water hammer oscillation, and leak-off segment. Then, the three segments were analyzed by energy analysis and correlation analysis. The results indicated that, one aspect, the frequency range of water hammer oscillation spans from 0 to 0.65 Hz, considered as effective water hammer signal. The pre-shut-in and leak-off segment ranges from 0 to 0.35 Hz and 0—0.2 Hz respectively. Meanwhile, odd harmonics were manifested in water hammer oscillation segment, with the harmonic frequencies ranging approximately from 0.07 to 0.75 Hz. Whereas integer harmonics were observed in pre-shut-in segment, ranging from 6 to 40 Hz. The other aspect, the energy distribution of water hammer signals was analyzed in different frequency ranges. In 0—1 Hz, an exponential decay was observed in all three segments. In 1—100 Hz, a periodical energy distribution was observed in pre-shut-in segment, an exponential decay was observed in water hammer oscillation, and an even energy distribution was observed in leak-off segment. In 100—500 Hz, an even energy distribution was observed in those three segments, yet the highest magnitude was noted in leak-off segment. In this study, the effective frequency range and energy distribution characteristics of the field-sampled water hammer signals in different segments were sufficiently elucidated quantitatively and qualitatively for the first time, laying the groundwork for optimizing the filtering parameters of the field filtering models and advancing the accuracy of identifying downhole event locations.

1. Introduction

With the wide application of hydraulic fracturing, fracture diagnostics has become a pivotal and well-concerned research topic in contemporary unconventional reservoir development (Cipolla

* Corresponding author.
E-mail address: huxiaodong@cup.edu.cn (X.-D. Hu).

and Wright, 2000; Parkhonyuk et al., 2018a; Mahmoud et al., 2021). Water hammer fracture diagnosis is an easy-operation, economic, and real-time method for fracturing diagnosis, which relies on water hammer. Water hammer is a sudden pressure pulsation that occurs after the pump shutdown at the wellhead (Urbanowicz et al., 2021, 2023). Propagating along the wellbore, water hammer pressure wave will interact with the fractures and other downhole events (Parkhonyuk et al., 2018a, 2018b). These events, altering the water hammer characteristics, can be identified by water hammer diagnostics (Holzhausen and Gooch, 1985; Bogdan et al., 2016; Korkin et al., 2020). Currently, it has been successfully applied to identify fracture size and location (Hwang et al., 2017; Kabannik et al., 2018; Ma et al., 2019; Hu et al., 2022), evaluate the effectiveness of diversion (Bogdan et al., 2016; Parkhonyuk et al., 2018a, 2018b; Alobaid et al., 2022a, 2022b), and assess bridge plug failure and casing leakage (Panjaitan et al., 2018; Abdrazakov et al., 2019; Borisenko et al., 2020; Zeng et al., 2023).

In the application of water hammer diagnostics, the field-sampled water hammer signals are often disturbed by noise interference. To ensure the accuracy of water hammer diagnostics, the filtering algorithm is necessary to improve the quality of field-sampled water hammer signals. Clarifying the characteristics of complex field-sampled signal is the essential for establishing filtering algorithm and optimizing parameters, ensuring the high quality of water hammer signals. In the research on water hammer signal characteristics, the period, amplitude, attenuation rate, and duration are essential time-domain characteristics that are related to the drilling and completion parameters, the complexity of fractures network, oil and gas production, etc. (Carey et al., 2015; Ciezobka et al., 2016; Hwang et al., 2017; Iriarte et al., 2017; Rodionov et al., 2017; Dung et al., 2021; Luo et al., 2023). Usually, it is difficult to fully understand the characteristics to obtain the explicit filter parameters only by time-domain analysis, which is just one dimension of time and frequency domain analysis. Therefore, it is necessary to analyze frequency-domain characteristics of water hammer signals, which provides a basis for filtering specifically.

The frequency-domain analysis is a key step in characteristics research of water hammer signals. It has been widely used in the water hammer phenomenon in Reservoir-Pipe-Valve system (Aliabadi et al., 2020). Serving as a foundation for the frequency-domain analytical solution of water hammer, a time-domain model of water hammer, considering friction, is proposed to assess the effect of the friction model on the simulation accuracy by water hammer number (Wh) (Urbanowicz et al., 2023). The correlation between Laplace-domain (complex frequency-domain) and time-domain analytical solutions was elucidated. A Laplace-domain solution considering fluid-solid interaction was proposed. Meanwhile, the spectral characteristics and factors of the pressure signal were analyzed (Bayle et al., 2023; Bayle and Plouraboué, 2024). The frequency-domain analytical solutions of water hammer signal in R-P-V systems serve as references for water hammer diagnostics. However, the research cannot be directly applied to analyze the frequency-domain characteristics in field-sampled water hammer signals. This is due to the significant differences of the water hammer propagation environments between the R-P-V system and the wellbore-fracture-reservoir system in field fracturing treatment.

In petroleum engineering, frequency-domain characteristics of water hammer signals were studied primarily in resonance frequency. The multi-peak resonance frequency was described to predict the fracture size and conductivity, which are derived from water hammer signals sampled below 10 Hz in fracturing field (Dunham et al., 2017). On this basis, the resonance frequency and wave reflection were studied to determine the fractures geometry

and properties (Liang et al., 2017). Clark et al. (2018) explored the correlation between the resonance frequency of water hammer signal and downhole boundary conditions. Meanwhile, hydraulic pulse events exhibited consistent non-random frequencies (resonance frequency), with peaks from 0 to 5 Hz. The amplitude peak of the resonance frequency is related to fractures introduced, which was used to determine hydraulic length (Qiu et al., 2022). Periodic harmonic frequency noise was observed in field-sampled water hammer signal, and a predictive deconvolution and comb filter was proposed (Alobaid et al., 2022). Therefore, previous research can be summarized as primarily focusing on resonance frequency to determine fracture properties (see Table 1). There is a lack of research on the effective frequency range and energy distribution of field-sampled water hammer signals, resulting in a lack of basis for designing field filtering models, which significantly affects the accuracy of water hammer diagnostics.

Based on the field-sampled water hammer signals collected during an on-site test in Junggar Basin, the frequency range and energy distribution characteristics were clarified both quantitatively and qualitatively for the first time. Firstly, the signal was preprocessed by mean normalization and Hampel filter to remove spike noise and eliminate DC frequency components. Secondly, the signal was segmented according to treating pressure under different conditions, resulting in pre-shut-in, water hammer oscillation, and leak-off segment. Thirdly, the frequency range and energy distribution of each segment were elucidated by energy analysis, including Parseval's theorem, Energy Spectral Density (ESD), and Power Spectral Density (PSD), etc. Finally, we discussed and compared the differences and similarities in frequency range and energy distribution characteristics of the field-sampled water hammer signals across the different segments, including frequency range, energy magnitude, energy attenuation, harmonic frequency, and correlation. This study revealed different frequency range and energy distribution characteristics in different segments for the first time, which provides a basis for optimizing filtering parameters to establish the filtering models of field-sampled water hammer signals, ultimately enhancing the identification accuracy of downhole events.

2. Methodology

A comprehensive water hammer segmentation-energy analysis method was proposed to analyze the frequency-domain characteristics of water hammer signals. The method mainly includes 4 steps: first, the signal is preprocessed by Hampel filter and mean normalization; second, the signal is divided into three segments by various pumping stages; third, the energy spectral density is used to determine frequency range and energy distribution; fourth, if there is a standard waveform, the correlation analysis is performed (Fig. 1).

2.1. Preprocessing

To effectively and robustly suppress outliners in field-sampled water hammer signal, the Hampel filter was used to preprocess (Hampel, 1974). Assuming a discrete time series, where n denotes the discrete time point and x_n represents the signal value at that point. For each point, choose a window centered on that point, typically with a size of $2k + 1$, where k is the window radius. First, the median of the window is calculated:

$$med_i = median(x_{i-k}, x_{i-k+1}, \ldots, x_i, \ldots, x_{i+k}) \tag{1}$$

where med_i is the median of the window centered at x_i. Second, the median absolute deviation (MAD) within the window is computed:

Table 1
Progress in characteristic analysis of water hammer.

Group	Subgroup	Progress in characteristic analysis of water hammer	Reference
Time-domain characteristics	Period, amplitude, attenuation rate, duration	How the period, amplitude, and duration are affected by fracture friction.	Carey et al. (2015); Hwang et al. (2017)
		How the period, amplitude, attenuation rate and duration are affected by completion parameters.	Iriarte et al. (2017)
		The relationship between fracture network complexity and water hammer attenuation rate.	Ciezobka et al. (2016); Rodionov et al. (2017); Dung et al. (2021); Luo et al. (2023)
	Other waveform characteristics	The relationship between the magnitude of the first pressure pulse and the pumping injection parameters.	Wang et al. (2008); Iriarte et al. (2017); Dung et al. (2021)
		The relationship between the inclining pressure trend and leak-off duration.	Dung et al. (2021)
		How the water hammer waveform is affected by under sampling.	Wang et al. (2008)
Frequency-domain characteristics	Reservoir-pipe-valve system	A time-domain model of water hammer is proposed, serving as a basis for the frequency-domain analytical solution.	Urbanowicz et al. (2023)
		A Laplace-domain solution considering fluid-solid interaction.	Bayle et al. (2023); Bayle and Plouraboué (2024)
	Wellbore-fracture-reservoir system (fracturing field)	The multi-peak resonance frequency is described to predict the fracture size and conductivity.	Dunham et al. (2017)
		The resonance frequency and wave reflection were studied to determine the fracture geometry and properties	Liang et al. (2017)
		The correlation between downhole boundary conditions and resonance frequency, with resonance frequency between 0 and 5 Hz.	Clark et al. (2018)
		The amplitude peak of harmonic frequency is used to determine hydraulic length.	Qiu et al. (2022)
		Periodic harmonic frequency noise is observed.	Alobaid et al. (2022)
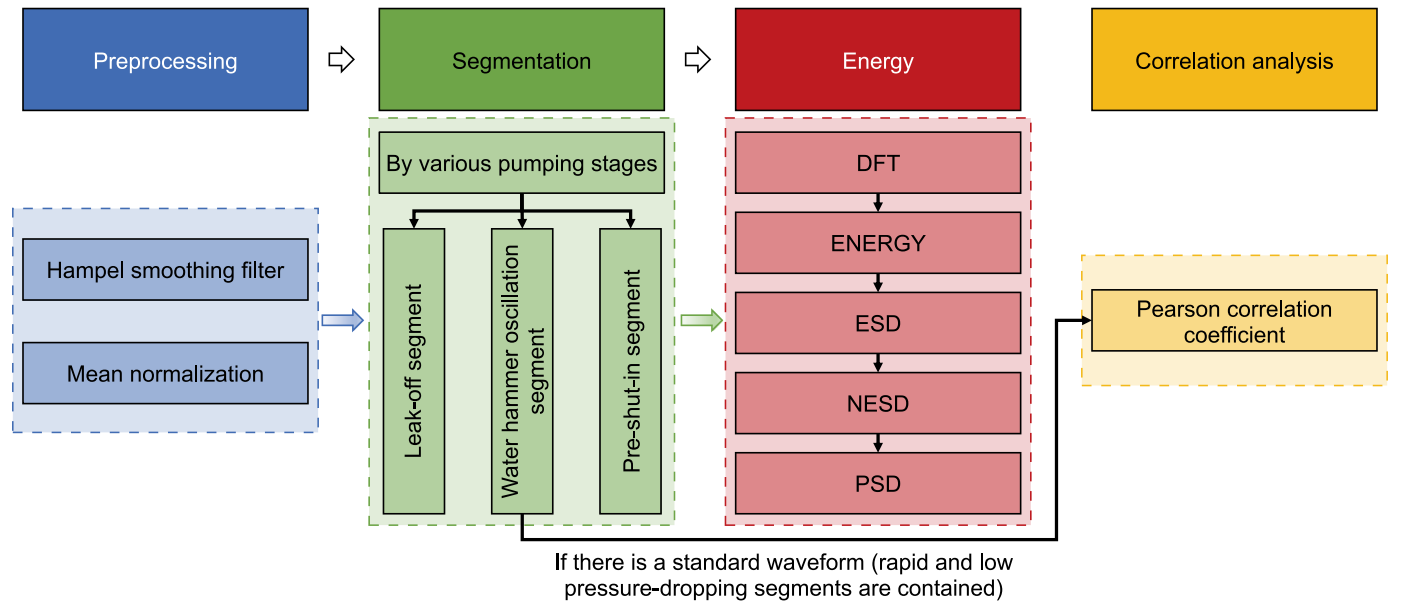
Fig. 1. The comprehensive water hammer segmentation-energy analysis method.

$$MAD_i = median\left(\left|x_j - med_i\right|\right), j \in \{i-k, i-k+1, \ldots, i, \ldots, i+k\} \quad (2)$$

Determine if the center data point x_i is an outlier, typically using a threshold factor t. If $\left|x_i - med_i\right| > t \cdot MAD_i$, then x_i is considered an outlier and is replaced with the median med_i; otherwise, it remains unchanged.

$$x_i = \begin{cases} x_i, \text{if } \left|x_i - med_i\right| \leq t \cdot MAD_i \\ med_i, \text{if } \left|x_i - med_i\right| > t \cdot MAD_i \end{cases} \quad (3)$$

To eliminate the DC frequency and remove irrelevant offsets of water hammer signals, mean normalization is used to standardize data by centering it around the mean (Ng and Jordan, 2002). First, the mean of the signal ($mean_n$) is calculated:

$$mean_n = \frac{1}{n} \sum_{i=1}^{n} x_i \quad (4)$$

where n is the length of the signal. Then center the data by subtracting the mean from each value to center the data around zero.

$$x_n' = x_n - mean_n \quad (5)$$

where x_n and x_n' are the original data and preprocessed data, respectively.

2.2. Segmentation

The water hammer pressure signal is divided into three

segments as objects: pre-shut-in segment, water hammer oscillation segment and leak-off segment, according to various pumping stages (Fig. 2). The pre-shut-in segment occurs before the pump shutdown, with pressure generated by the pump's constant-speed liquid injection. The water hammer oscillation segment occurs at the moment of pump shutdown. The water hammer wave generated by the sudden shutdown or pressure reduction, propagating along the wellbore and containing the information of downhole events. The leak-off segment occurs when water hammer oscillation attenuates to zero.

2.3. Energy spectral density analysis

The calculation method for the energy spectral density of discrete-time signals was systematically presented by Oppenheim et al. (1983). It was employed to analyze the frequency range and energy distribution of field water hammer signals in various pumping stages. Assuming a discrete time series, where n denotes the discrete time point and $x[n]$ represents the signal value at that point. The discrete-time Fourier transform (DFT) is utilized to transform $x[n]$ into the frequency domain.

$$X[k] = \sum_{n=0}^{N-1} x[n] e^{-j2\pi kn/N} \tag{6}$$

where $X[k]$ is the DFT coefficient, N is the length of $[n]$, j represents the imaginary unit, and k is frequency index. According to Parseval's theorem:

$$E = \sum_{n=0}^{N-1} |x[n]|^2 = \frac{1}{N} \sum_{k=0}^{N-1} |X[k]|^2 \tag{7}$$

where E is the total energy of $x[n]$, it can be calculated in time domain and frequency (Eq. (7)). The energy spectral density (ESD) is the signal energy in the unit frequency, representing the energy distribution in the frequency domain. The ESD can be calculated by taking the square of the modulus of DFT.

$$ESD[k] = |X[k]|^2 \tag{8}$$

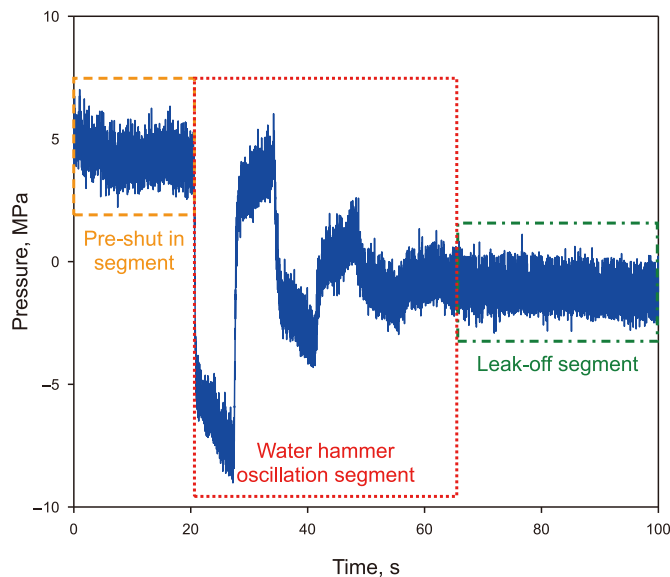where $ESD[k]$ represents the ESD at frequency index k (dB). When the frequency index k denotes the interval $[k_{\min}, k_{\max}]$, where $k_{\min} \geq 0$, it can be written as:

$$ESD_{\text{band}} = \sum_{k_{\min}}^{k_{\max}} |X[k]|^2 \tag{9}$$

where ESD_{band} represents the ESD at frequency interval $k_{\max} - k_{\min}$ (dB). Other calculation methods remain unchanged and will not be elaborated upon. The normalized energy spectral density (NESD) normalizes ESD to a percentage of energy within a unit. It can be calculated as:

$$NESD[k] = \frac{ESD[k]}{\sum_{k=0}^{N-1} ESD[k]} \tag{10}$$

where $NESD[k]$ denotes the normalized energy spectral density at k (%). The power spectral density (PSD) represents the power distribution of the signal in frequency domain. PSD is computed as the average value of ESD.

$$PSD[k] = \frac{1}{N} \left| \sum_{n=0}^{N-1} x(n) e^{-j2\pi nk/N} \right|^2 = \frac{1}{N} ESD[k] \tag{11}$$

where $PSD[k]$ denotes the PSD at k (dB). Typically, PSD is represented as a logarithmic scale. In the derivation of the above formula, k is the frequency index, it can be converted to the actual frequency:

$$f = \frac{k}{N}, k = 0, 1, \ldots, N-1 \tag{12}$$

$$f_{\text{actual}} = f \times F_s \tag{13}$$

where f is the normalized frequency, F_s is the sampling frequency, and f_{actual} is the actual frequency. In this paper $F_s = 1000$ Hz. The frequency range of water hammer signal can be calculated by ESD, NESD, and PSD.

2.4. Correlation analysis

Introduced by Karl Pearson in 1896, the Pearson correlation coefficient is utilized to measure the linear relationship between two variables (Pearson, 1896). Ott et al. further introduced the application of this method (Ott and Longnecker, 2016). In this paper, it was used to measure the correlation of pressure-dropping segments within water hammer oscillation, if there is a standard waveform contained rapid and slow pressure-dropping segments. Assuming two discrete time series, where n denotes the discrete time point, $x[n]$ and $y[n]$ represents the signal value at that point in two series. The Pearson correlation coefficient is calculated by:

$$\rho_{xy} = \frac{\text{cov}(x, y)}{\sigma_x \sigma_y} \tag{14}$$

where $\text{cov}(x, y)$ is the covariance of $x[n]$ and $y[n]$, σ_x and σ_y denote the standard deviation of $x[n]$ and $y[n]$, and ρ_{xy} is the Pearson correlation coefficient of $x[n]$ and $y[n]$. ρ_{xy} ranges from -1 to 1. If $\rho_{xy} > 0$, it indicates positive correlation; if $\rho_{xy} < 0$, it signifies negative correlation; if $\rho_{xy} = 0$, no linear correlation is implied; if $\rho_{xy} = 1$, complete linear correlation is implied.

3. Analysis and discussion

Fig. 2. Field sampled water hammer signal and its segmentation (e.g. Stage2).

An on-site test was carried out in a horizontal well in the
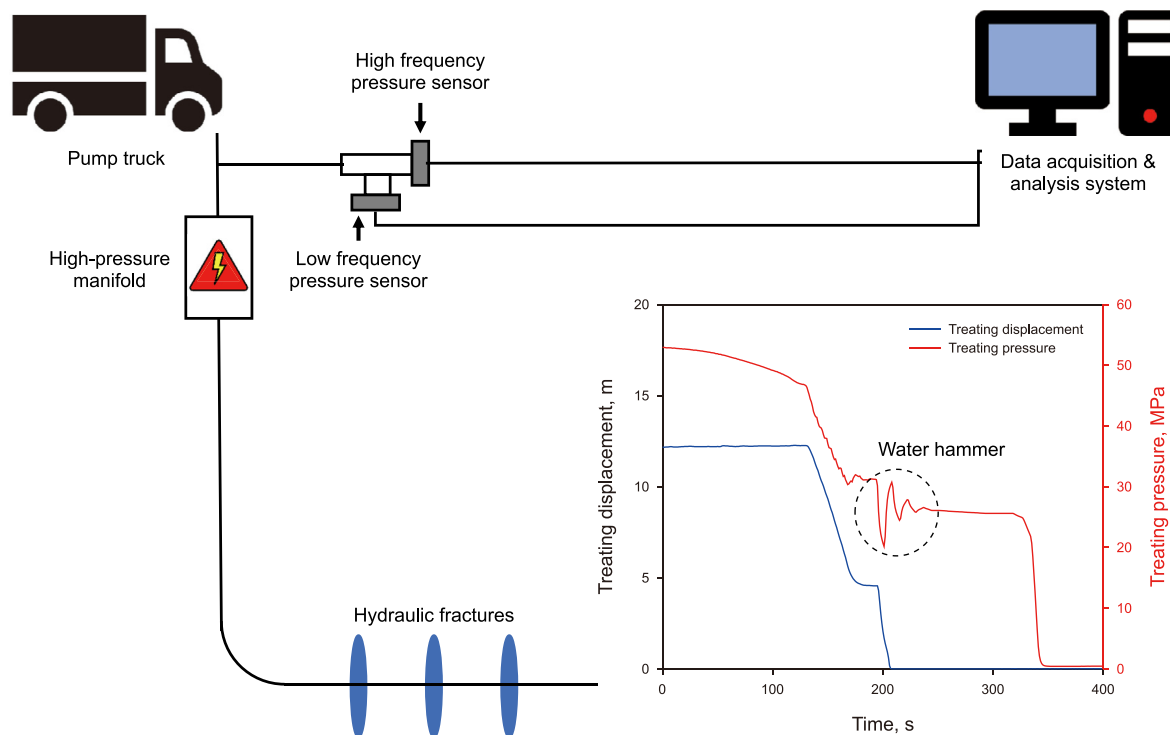
Fig. 3. The equipment layout. The high-frequency pressure sensor and the low-frequency pressure sensor are linked to the data acquisition and analysis system. At the other end, they are respectively connected to the three-way valve. The other end of three-way valve is connected to the downhole fractures through the high-pressure manifold.
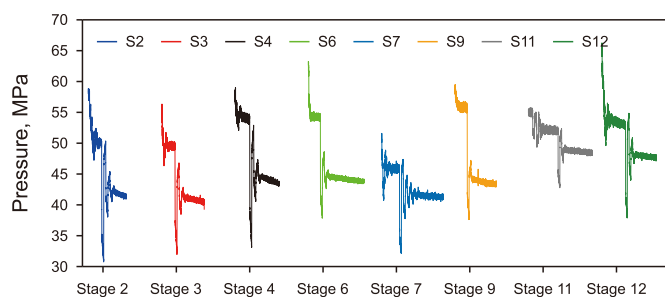
**Fig. 4.** Field sampled water hammer signals.

Junggar Basin by staged fracturing technique. Staged fracturing technique was adopted by Well A, with 14 stages being divided. The maximum deviation depth of Well A is 5132 m, with a horizontal stage length of 1066 m. A high-frequency pressure sensor was placed at the wellhead to sample water hammer data during the fracturing treatment. Monitoring was performed throughout the hydraulic treatment. To capture the entire water hammer waveform, the water hammer data was sampled at 1000 Hz. The general location configuration, including high frequency pressure sensor, data acquisition and analysis system is shown in Fig. 3.

In this paper, 8 stages with better water hammer quality (as shown in Fig. 4) were selected for research based on the integral water hammer waveform. The selected fracturing stages were stage
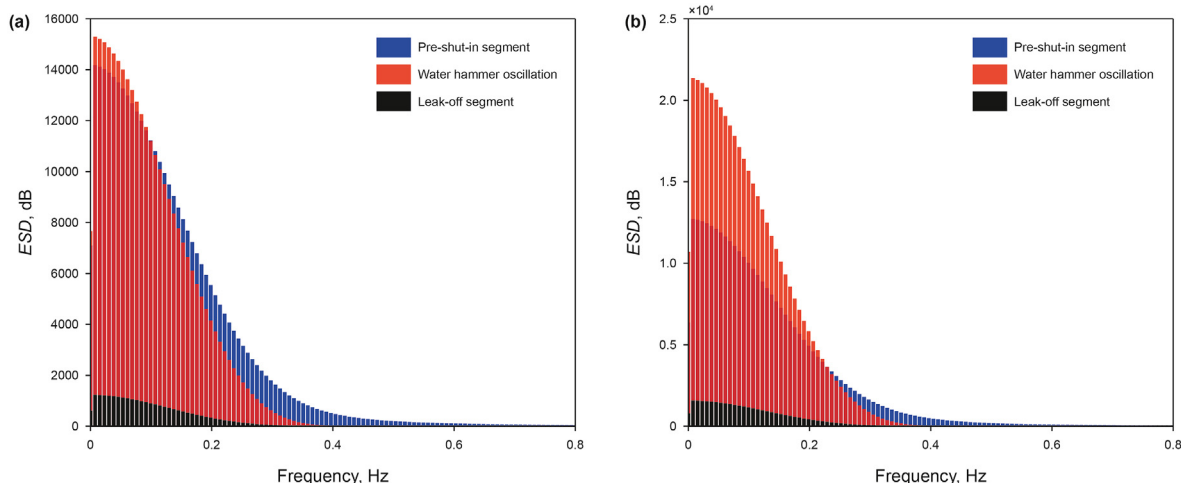
Fig. 5. *ESD* of pre-shut-in, water hammer oscillation, and leak-off segment (**a**) Stage 2; (**b**) Stage 4.
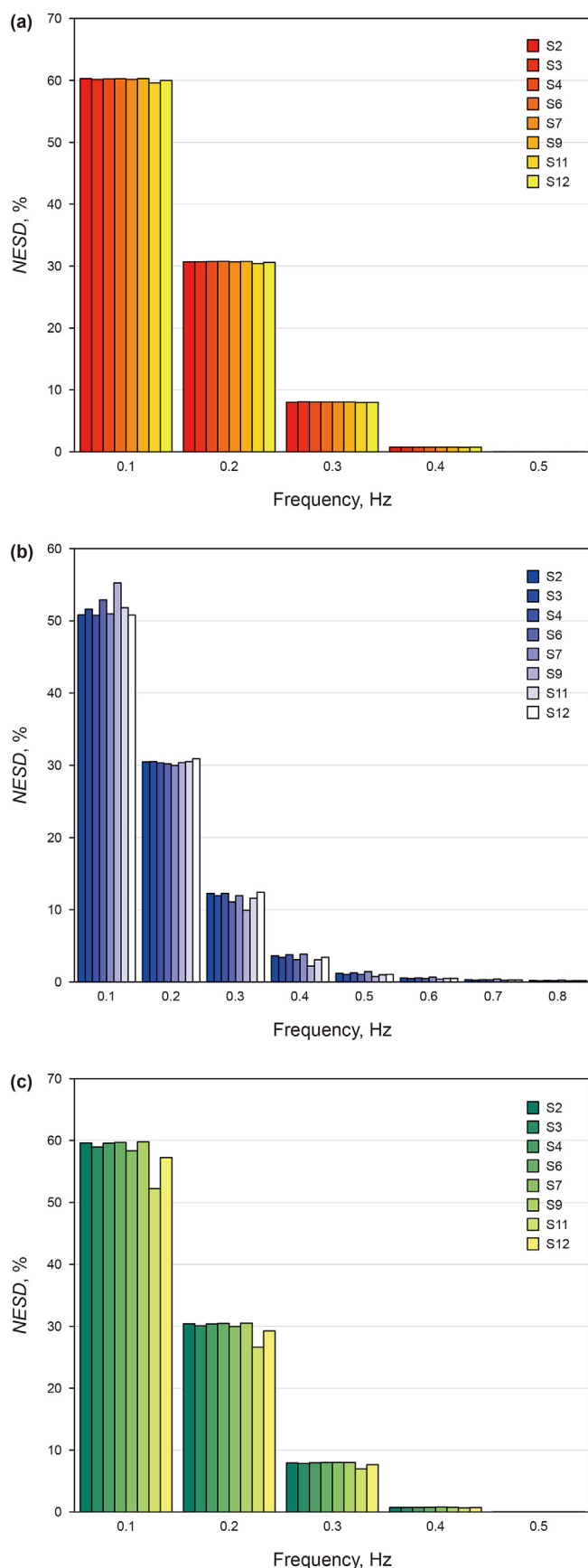
Fig. 6. *NESD* of pre-shut-in, water hammer oscillation, and leak-off segment (all stages): (**a**) Pre-shut-in segment; (**b**) Water hammer oscillation segment; (**c**) Leak-off segment.

2, stage 3, stage 4, stage 6, stage 7, stage 9, stage 11, and stage 12. The corresponding bridge plug seals were located at depths of 4973, 4917, 4857, 4717, 4637, 4459, 4287, and 4197 m, respectively. Firstly, the water hammer signals were preprocessed by data cleaning and averaging. Data from 80 s after the pump shutdown, along with the previous 20 s, were intercepted for analysis. The Hampel filter and mean normalization were used to preprocess the intercepted signal (Eqs. (1–5)). Finally, the energy spectral density method was used to clarify the frequency range and energy distribution in high frequency (1–500 Hz) and low frequency (less than 1 Hz), as well as pressure-dropping segment within water hammer signals.

3.1. Characteristics of pre-shut-in, water hammer oscillation, and leak-off in low frequency

The frequency range of pre-shut-in, water hammer oscillation, and leak-off segment was analyzed by *ESD* (Fig. 5) (Eq. (8)). When the energy within per unit (0.01 Hz) is less than 0.1% of the total energy of the signal, the signal energy is deemed to be zero (Not *NESD*). The frequency range of water hammer oscillation spans from 0 to 0.65 Hz, considered as effective water hammer signal. Whereas pre-shut-in ranges from 0 to 0.35 Hz, and leak-off extends from 0 to 0.2 Hz. Therefore, varying frequency ranges were observed in different segments of pumping stages in water hammer signals. This is because the different segments, defined by treating pressure under varying conditions, originate from distinct signal sources. In the pre-shut-in segment, the frequency and energy contributions primarily come from the pump. During water hammer oscillation, the frequency and energy are mainly driven by the water hammer phenomenon occurring between the wellbore and fracture at pump shutdown. In the leak-off segment, the frequency and energy contributions primarily stem from environmental noise and inherent system noise.

The *NESD* of pre-shut-in, water hammer oscillation, and leak-off segment was calculated with a 0.01 Hz interval (Fig. 6) (Eq. (10)). Initially, consistency in the *NESD* of pre-shut-in, water hammer oscillation, and leak-off is observed across 8 stages, respectively. When the *NESD* is less than 0.02%, the energy proportion is deemed to be zero. In pre-shut-in, the energy within the range of 0–0.4 Hz accounts for more than 98% of the segment. The energy proportions of 0–0.1, 0.1–0.2 0.2–0.3, and 0.3–0.4 Hz are 60%, 30%, 8%, and 0.75%, respectively. In water hammer oscillation, the energy within the range of 0–0.6 Hz accounts for more than 97% of the segment. The energy proportions of 0–0.1, 0.1–0.2, 0.2–0.3, 0.3–0.4, 0.4–0.5, and 0.5–0.6 Hz are 51%–55%, 30%, 11%, 3%, 1%, and 0.5%, approximately. In leak-off, the energy within the range of 0–0.4 Hz accounts for more than 96% of the segment. The energy proportions of 0–0.1, 0.1–0.2, 0.2– 0.3, and 0.3–0.4 Hz are 59%, 30%, 7.5%, and 0.7%, approximately. The research indicated that the water hammer signal is primarily distributed in the range of less than 0.7 Hz, with more than 96% of the total energy attributed to this range. Therefore, the main frequency range of water hammer signal is 0–0.7 Hz.

Treating pressure, also known as wellhead pressure or fracturing pressure, is the pressure observed when liquid is pumped through pipelines and fracturing equipment during hydraulic fracturing. The relationship between the total energy of water hammer signals (Eq. (7)) and treating pressure was analyzed, indicating a positive correction (Fig. 7(a)). Treating displacement refers to the volume of liquid pumped downhole during hydraulic fracturing. The relationship between the energy of water hammer oscillation segment (E_w) (Eq. (7)) and treating displacement was analyzed, demonstrating a positive correction overall (Fig. 7(b)). The range of treating displacement is 3.5–4.5 m³/min, and the range of the energy of water hammer oscillation is 5×10^4 to
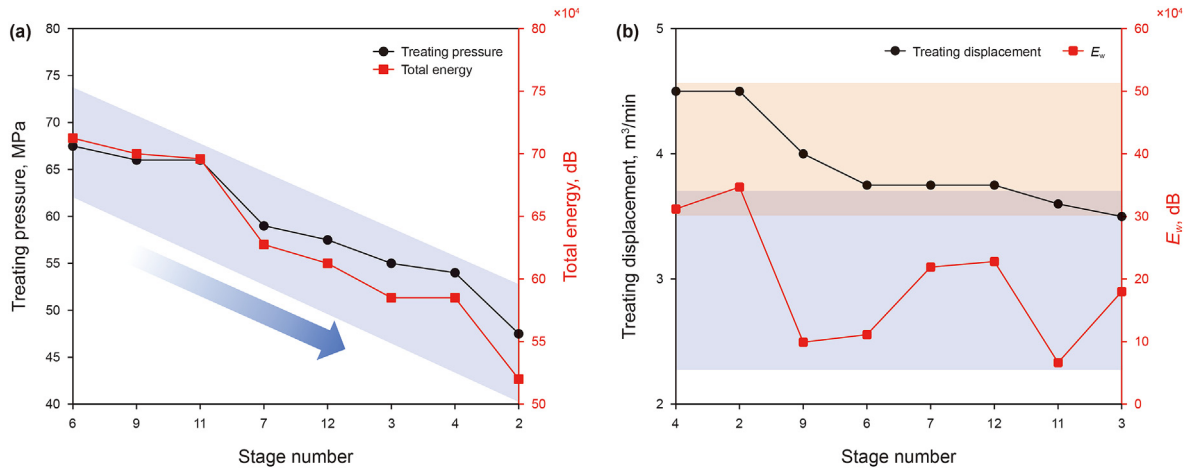
Fig. 7. The relationship between signal energy and pump parameters: (**a**) The relationship between the total energy of water hammer signals and treating pressure; (**b**) The relationship between the energy of water hammer oscillation segment (E_w) and treating pressure.

35×10^4 dB. Therefore, the energy of water hammer signal is influenced by the pumping parameters. The higher treating displacement and treating pressure, the greater amplitude of water hammer oscillation, resulting the stronger energy.

The relative energy magnitude of different segments was analyzed (Fig. 8). The energy of pre-shut-in is denoted as E_p, the energy of water hammer oscillation is denoted as E_w, and the energy of leak-off is denoted as E_l (Eq. (7)). The relative energy magnitude between E_p, E_w, and E_l was analyzed by comparing the average pressure of pre-shut-in (P_p) and the maximum reflection

pressure of water hammer oscillation (P_w) (Fig. 9). The result indicated that E_l is the smallest among E_p, E_w, and E_l. Additionally, the relative magnitude of E_p and E_w is determined by the relative magnitude of P_p and P_w. When $P_p > P_w$, $E_p > E_w > E_l$; when $P_w > P_p$, $E_w > E_p > E_l$; when $P_p \approx P_w$, $E_p \approx E_w > E_l$.

Therefore, the relative energy magnitude of different segments is associated with the relative magnitude of P_p and P_w.

The harmonic frequencies of different segments were analyzed

$$\begin{cases} E_p(s) > E_w(s) > E_l(s), & P_p(s) > P_w(s) \\ E_w(s) > E_p(s) > E_l(s), & P_p(s) < P_w(s) \\ E_p(s) \approx E_w(s) > E_l(s), & P_p(s) \approx P_w(s) \end{cases}, \quad \text{where} \quad s = 2, 3, 4, 6, 7, 9, 11, 12 \tag{15}$$
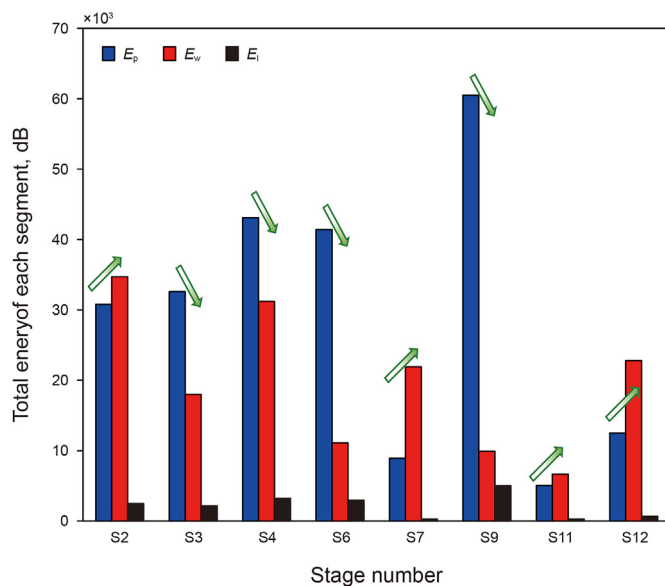
Fig. 8. The total energy of different segments (all stages).

by *PSD* (Fig. 10) (Eq. (11)). It was shown that a periodic frequency exists in the pre-shut-in, originating from the pump noise. The harmonic frequencies of the pre-shut-in of all stages were counted (Table 2) (Fig. 11). An integer harmonic relationship, along with the harmonic relationship of two fundamental frequencies were observed in the pre-shut-in of all stages. Group 1 includes stage 2, stage 3, stage 4, stage 9 and stage 12, with a fundamental frequency of 6.65 Hz and its integer harmonic frequencies. Stage 9 is considered to belong to Group 1, but there is a little error. Group 2 consists of stage 6, with a fundamental frequency of 9.3 Hz and its integer harmonic frequency. Additionally, stage 7 and stage 11 exhibit both the fundamental frequency of 6.65 Hz and 9.3 Hz.

The harmonic frequency of water hammer oscillation was analyzed by *DFT* (Fig. 12) (Eq. (6)). It was shown that odd harmonics were manifested in water hammer oscillation segments. The harmonic frequencies of the water hammer oscillation of all stages were counted (Fig. 13). It was shown that the harmonic frequency ranges from 0.07 to 0.75 Hz, which is similar to the frequency range of the water hammer oscillation depicted in Fig. 5.
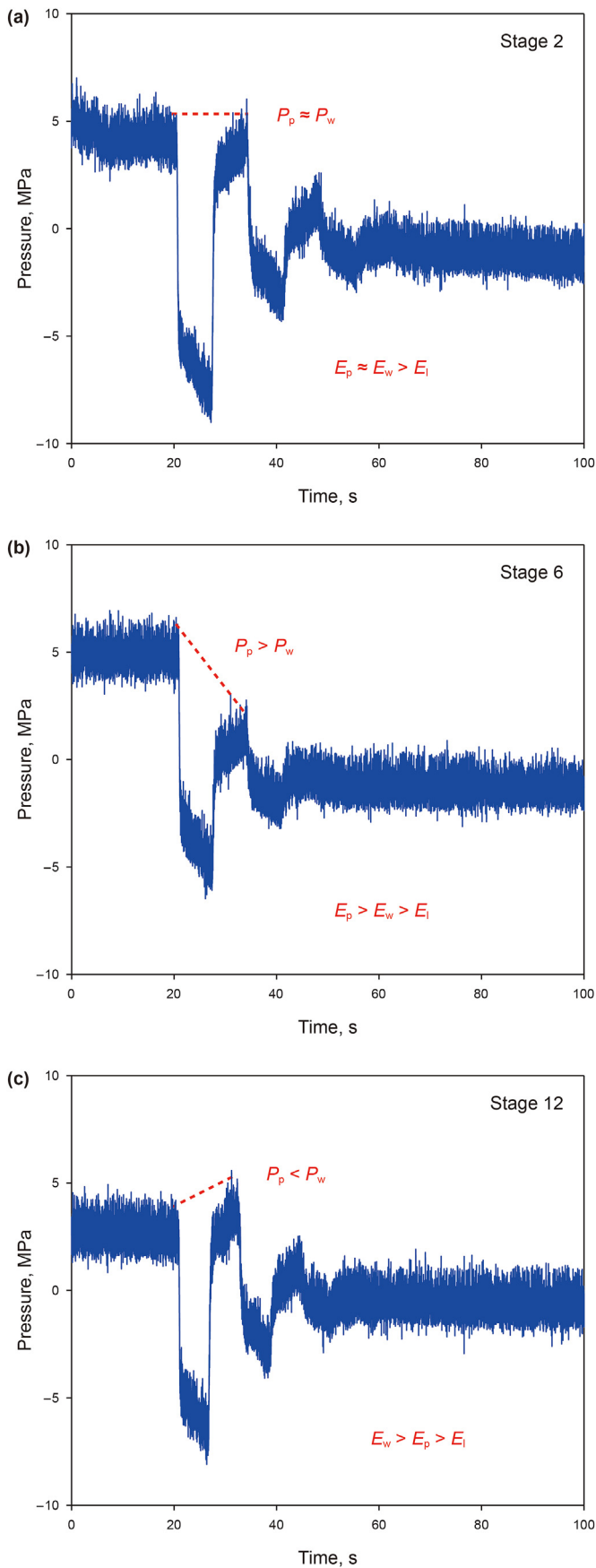
Fig. 9. The relative magnitude of P_p and P_w: (**a**) Stage 2; (**b**) Stage 6; (**c**) Stage 12.
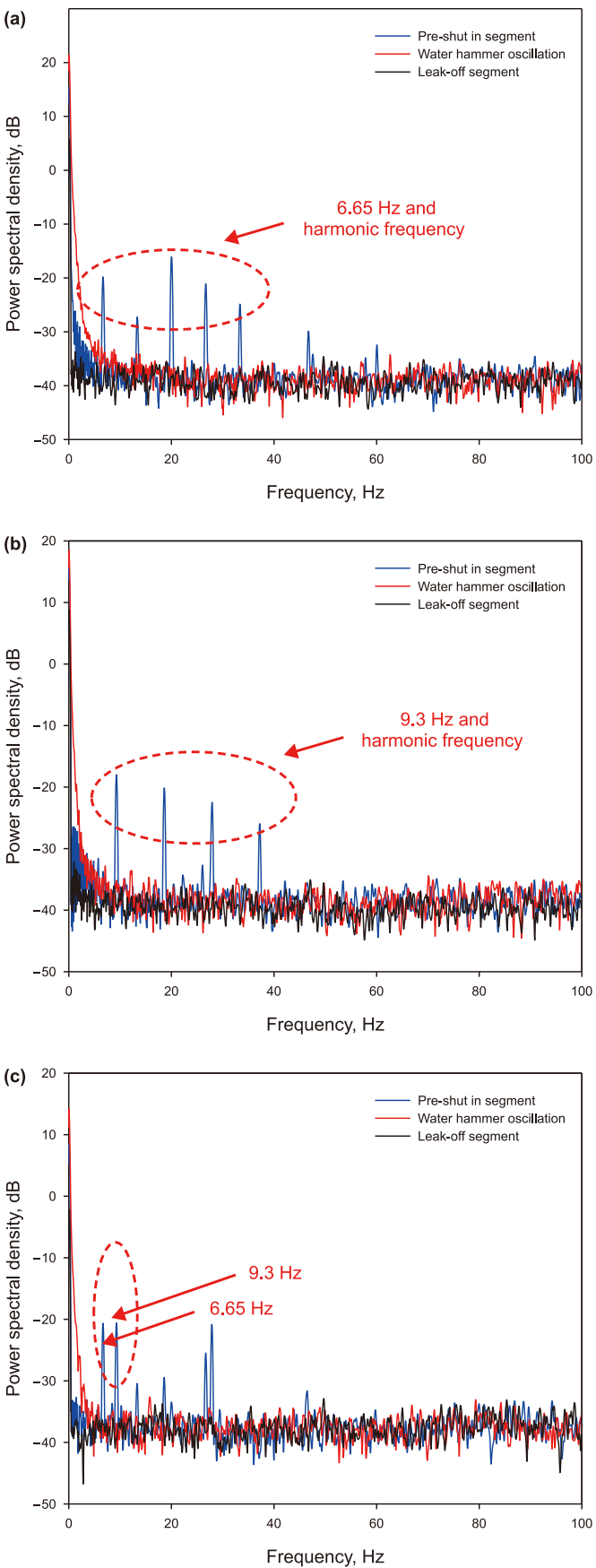
Fig. 10. *PSD* of pre-shut-in, water hammer oscillation, and leak-off: (**a**) Stage 2; (**b**) Stage 6; (**c**) Stage 11.

Table 2
Harmonic frequencies of pre-shut-in segment.

Stage number	Harmonic frequencies						
Stage 2	6.65	13.35	20.05	26.7	33.35		
Stage 3	6.65	20	26.65	33.35			
Stage 4	6.65	13.3	19.95	26.7			
Stage 6	9.3	18.6	27.95	37.2			
Stage 7	6.65	9.3	18.6	20	26.7	27.9	37.2
Stage 9	6.3	13.35	18.95	25.25	31.6		
Stage 11	6.65	9.3	13.35	18.6	26.7	27.9	
Stage 12	6.7	13.35	20.05	26.75	33.35		

3.2. Characteristics of pre-shut-in, water hammer oscillation, and leak-off in high frequency

The energy of the relatively high-frequency (more than 1 Hz) constitutes less than 5% of the total energy of water hammer signal. Therefore, it is defined as the secondary frequency range of the water hammer signal. The signal of the 1–500 Hz frequency of the water hammer signal was displayed (Fig. 14). The high-frequency signal was divided by the segmentation method outlined in Section 3.1.

The energy of water hammer signals within the frequency ranges of 1–100, 100–200, 200–300, 300–400, and 400–500 Hz was calculated respectively (Fig. 15) (Eq. (7)). It was shown that the energy within 1–100 Hz is the strongest, exceeding 1×10^3 dB. The energy distribution within 100–200, 200–300, 300–400, and 400–500 Hz of all stages is relatively uniform. However, abnormalities were observed in stage 7. The energy within each frequency band is less than 1×10^3 dB, which is lower than that of 1–100 Hz. The object in the high-frequency was divided into two frequency range: 1–100 Hz and 100–500 Hz.

The NESD of pre-shut-in, water hammer oscillation, and leak-off within 1–100 Hz was analyzed (Fig. 16) (Eq. (10)). The NESD of stage 4 was shown as Fig. 16(a), and the NESD of all stages was shown as Fig. 16(b). A statistical law was shown, with similar patterns observed in 8 stages. The results indicated that the maximum energy of pre-shut-in is primarily attributed to the periodic harmonic noise, which aligns with the findings depicted in Fig. 10. Besides, the NESD of water hammer oscillation is exponentially decaying. When the frequency surpasses 5 Hz, the energy of water hammer oscillation is nearly attenuated to zero. Additionally, the energy
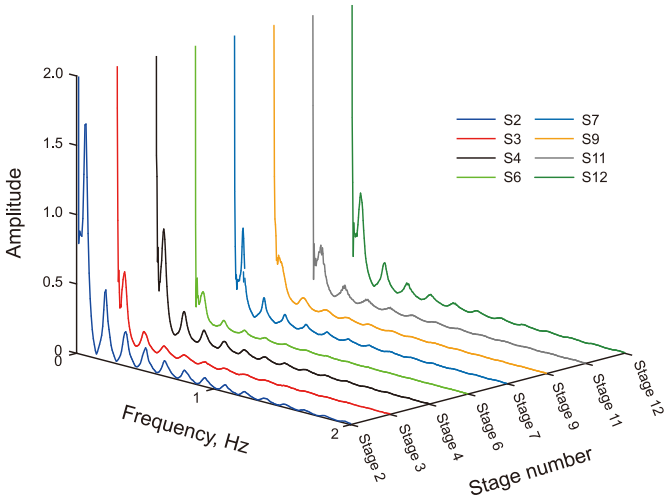

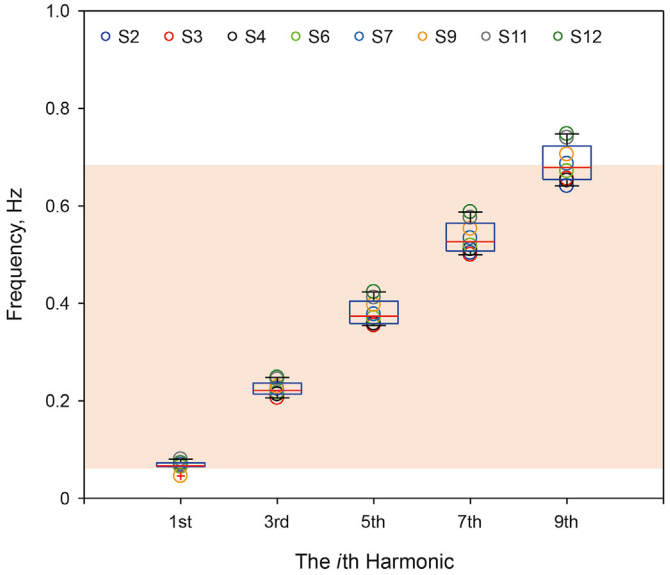**Fig. 12.** The spectrum of water hammer oscillation segments.

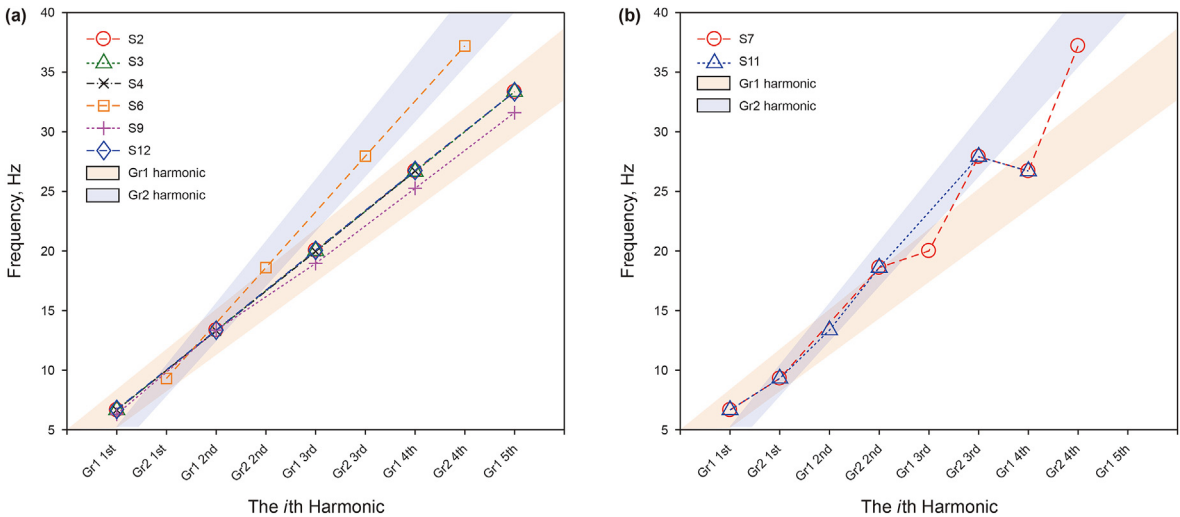**Fig. 13.** Statistics of harmonic frequencies of water hammer oscillation segments.

Fig. 11. Statistics of harmonic frequencies of pre-shut-in segments: (**a**) S2, S3, S4, S6, S9, S12; (**b**) S7, S11.
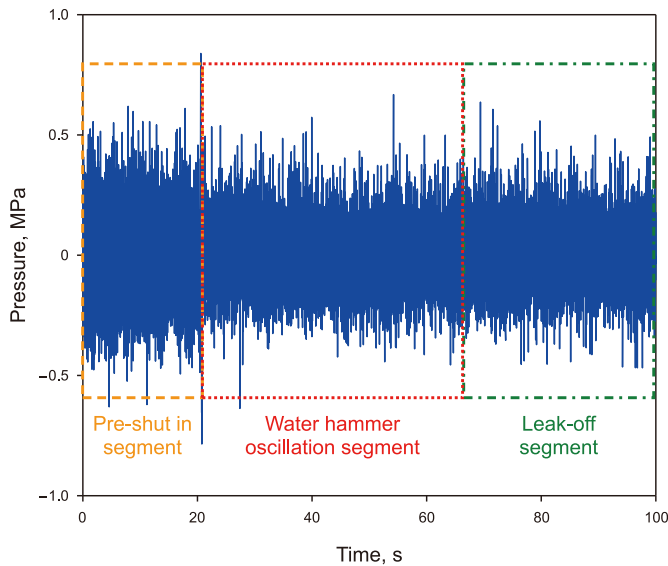
Fig. 14. High-frequency signal of water hammer signal (e.g. stage 2).
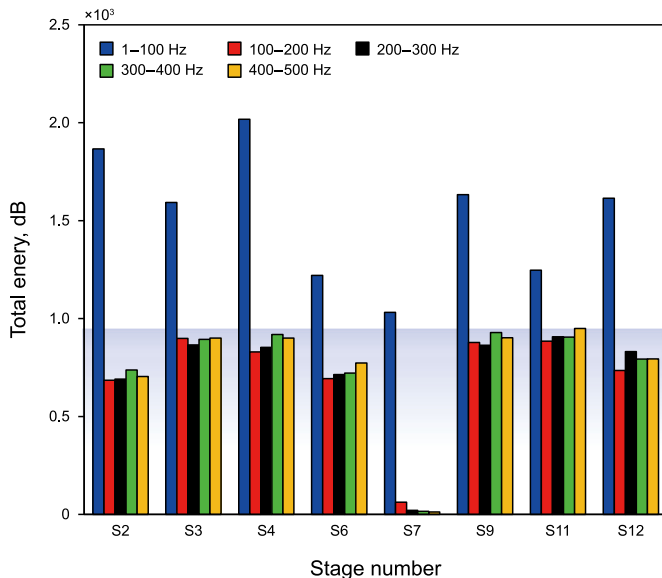

Fig. 15. The energy of water hammer signals within the frequency ranges of 1–100, 100–200, 200–300, 300– 400, and 400–500 Hz.

distribution of leak-off within 1–100 Hz is relatively uniform.

The *NESD* of pre-shut-in, water hammer oscillation, and leak-off within 100–500 Hz was analyzed (Fig. 17) (Eq. (10)). A statistical law is shown, with similar patterns observed in 8 stages. It was shown that the energy proportion of pre-shut-in, water hammer oscillation, and leak-off exhibited relative uniformity within 100–500 Hz. The energy proportion of leak-off is the highest, while that of pre-shut-in and water hammer oscillation is similar. This is because the total energy is constant, the relative energy is stronger at high frequency, whereas weaker at low frequency.

3.3. Characteristics of pressure-dropping segment within water hammer oscillation

The water hammer oscillation is considered more complex than the pre-shut-in and leak-off. Water hammer oscillation is emphasized in diagnostics because it contains important fracture responses. According to the pressure drop rate in each period, the water hammer oscillation (Fig. 18(a)) can be divided into two segments: rapid pressure-dropping segment and slow pressure-dropping segment (Fig. 18(b)). Firstly, the slow pressure-dropping segment was studied, which is denoted as $P_1, P_2...P_n$ (Fig. 18(c)). Secondly, the pressure-dropping segment combined with slow pressure-dropping and fast pressure-dropping segment was studied, which is denoted as $P_1', P_2'...P_n'$ (Fig. 18(d)).

The *ESD* and *NESD* of slow pressure-dropping segment of all stages were calculated (Eq. (8) and Eq. (10)). The *ESD* of stage 2 was shown as Fig. 19, and the *NESD* of P_1 within all stages was shown as Fig. 20. The energy of $P_1, P_2...P_n$ are denoted as $E_{P_1}, E_{P_2}...E_{P_n}$. It was shown that the frequency range of slow pressure-dropping segment ranges from 0 to 1.2 Hz. Meanwhile, $E_{P_1}, E_{P_2}...E_{P_n}$ exhibits an overall attenuation pattern. In addition, the *NESD* of slow pressure-dropping segment within all stages is similar.

The correlation between $P_1, P_2...P_n$ was analyzed by Pearson correlation coefficient (Eq. (14)), resulting in the correlation coefficient heatmap of $P_1, P_2...P_n$ (Fig. 21). The correlation coefficient between P_1 and $P_i (0 < i < n)$ of all stages were calculated (Fig. 22). Overall, high correlation was observed among slow pressure-dropping segments, with correlation coefficient exceeding 0.7. Simultaneously, as time goes on (the duration of water hammer signal), the correlation among each pressure-dropping segment shows a decreased trend. This phenomenon may be attributed to the increasing complexity and differences of waveform oscillations as the signal decays.

The correlation between $P_1', P_2'...P_n'$ was analyzed by Pearson correlation coefficient (Eq. (14)), resulting in the correlation coefficient heatmap of $P_1', P_2'...P_n'$ (Fig. 23). Compared with Fig. 21, the correlation with P_i' and P_{i+1}' is enhanced, with correlation exceeding 0.9. Therefore, it is considered that the rapid pressure-dropping segment contains valid information.

4. Conclusions

This paper analyzed the field-sampled water hammer signals from 8 stages in a horizontal well, comparing high frequency (1–500 Hz), low frequency (≤ 1 Hz), and pressure dropping segment. Key characteristics such as frequency range, energy distribution, harmonic frequency, and correlation were examined. The conclusions are as follows.

(1) The effective frequency range of field-sampled water hammer signal was determined by segmentation-energy analysis. The water hammer oscillation spans from 0 to 0.65 Hz, considered as effective signal. The pre-shut-in segment ranges from 0 to 0.35 Hz, while leak-off segment extends from 0 to 0.2 Hz. Meanwhile, water hammer oscillation exhibits odd harmonics ranging from 0.07 to 0.75 Hz. Whereas pre-shut-in segment exhibits integer harmonics ranging from 6 to 40 Hz. Different frequency ranges are associated with specific segments of pumping stages.

(2) The energy distribution was revealed within 0–1, 1–100, and 100–500 Hz. In 0–1 Hz, exponential decay was exhibited in
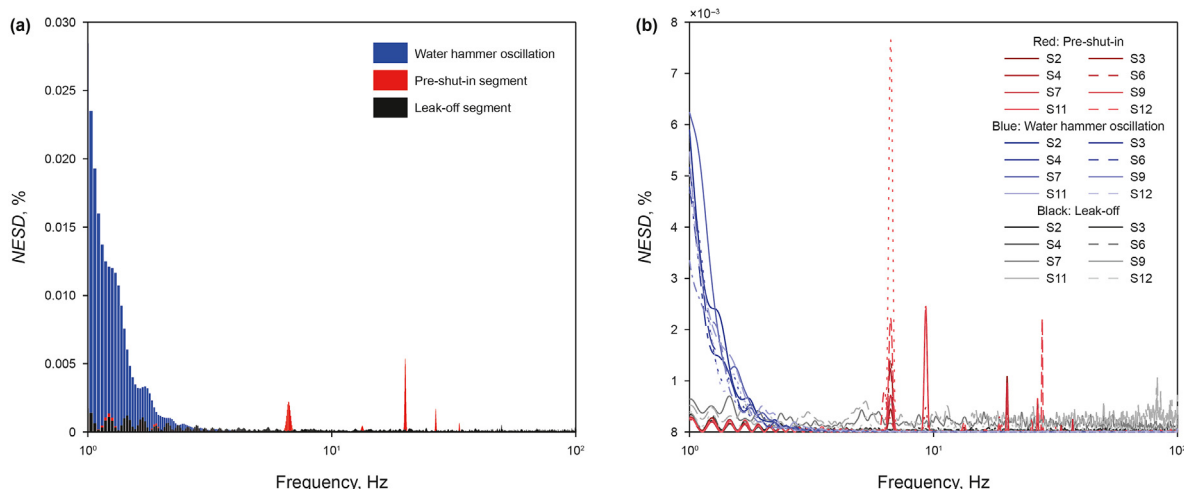
Fig. 16. *NESD* of pre-shut-in, water hammer oscillation, and leak-off within 1—100 Hz: (**a**) Stage 4; (**b**) All stages.
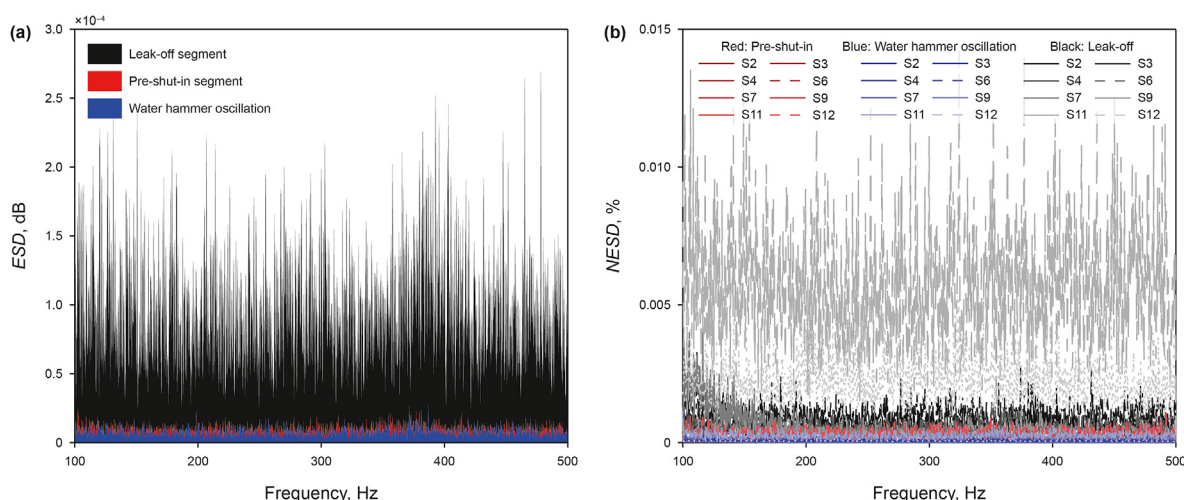

Fig. 17. *NESD* of pre-shut-in, water hammer oscillation, and leak-off within 100—500 Hz: (**a**) Stage 4; (**b**) All stages.

pre-shut-in, water hammer oscillation, and leak-off. In 1—100 Hz, the dominant energy in pre-shut-in segment is attributed to harmonic frequencies, exponential decay was presented in water hammer oscillation, and an even energy distribution was noted in leak-off. In 100—500 Hz, all segments show even energy distribution. Different energy distributions are related to the information contained in different segments of water hammer signals.

(3) The correlation among each pressure-dropping segment within water hammer oscillation was elucidated by Pearson correlation coefficient. As the duration goes on, the correlation gradually decreases. Meanwhile, the frequency range of each pressure-dropping segment consistently spans from 0 to 1.2 Hz. Moreover, the energy of water hammer signal was positively correlated with treating pressure and displacement.

(4) This study clarified the frequency-domain characteristics of field-sampled water hammer signals, which provides a basis for specifically filtering parameters setting, including frequency range, energy threshold, filter type and order, laying the groundwork for establishing the field filtering models and advancing the accuracy of identifying downhole event locations. The comprehensive water hammer segmentation-energy analysis method can be utilized to identify the characteristics of water hammer signals in various scenarios, including pre- and post-diversion, casing leakage, etc.

(5) This study identifies a narrow frequency range and rapid exponential energy decay in field-sampled water hammer signals, which pose significant challenges for signal processing, including limitations in filter attenuation speed and bandwidth for fine filtering. This finding imposes stricter requirements on designing filter, offering critical directions for future research and improvements.

CRediT authorship contribution statement

Ya-Jing Wang: Writing — original draft, Software, Methodology, Conceptualization. **Xiao-Dong Hu:** Supervision. **Fu-Jian Zhou:** Supervision. **Pu-Kang Yi:** Writing — review & editing, Conceptualization. **Wei-Peng Guan:** Software. **Yang Qiu:** Writing — review & editing, Conceptualization. **En-Jia Dong:** Data curation. **Peng-Tian Zhang:** Validation.
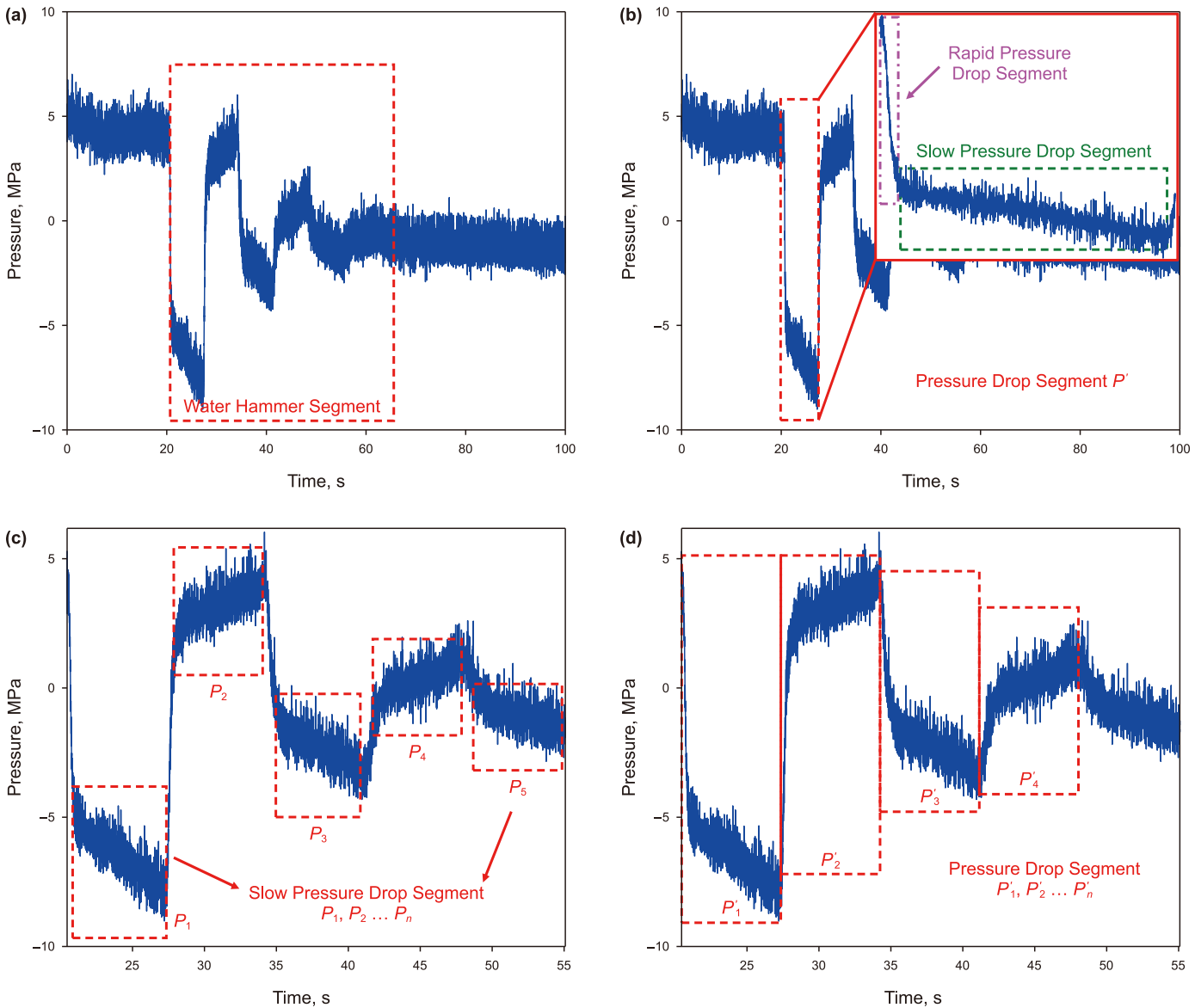
Fig. 18. The schematic diagram of pressure-dropping segment within water hammer oscillation. (**a**) Water hammer oscillation; (**b**) Rapid pressure-dropping and slow pressure drop segment; (**c**) The schematic diagram of slow pressure-dropping and its number; (**d**) The schematic diagram of pressure-dropping segment and its number.
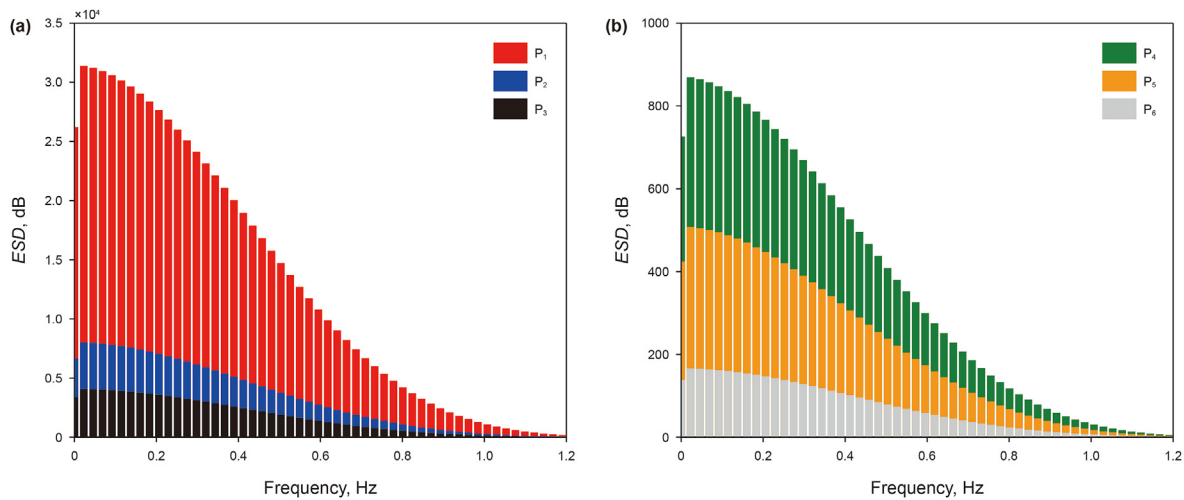
Fig. 19. The *ESD* of $P_1, P_2, ..., P_n$ within stage 2: (**a**) P_1, P_2, P_3; (**b**) P_4, P_5, P_6.
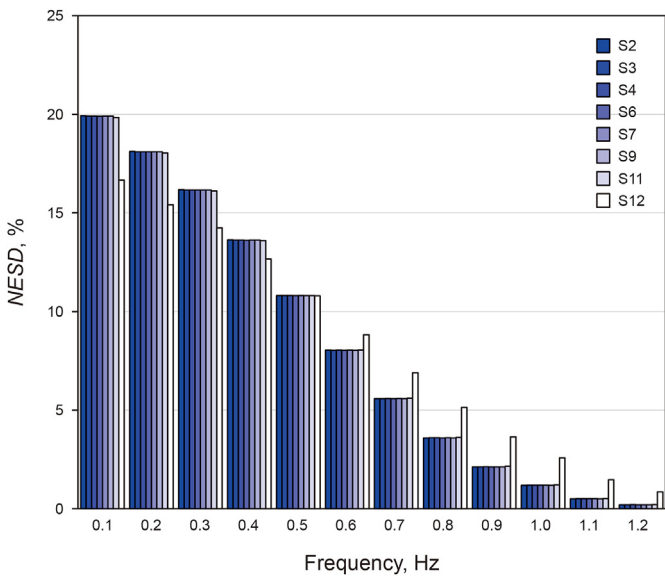

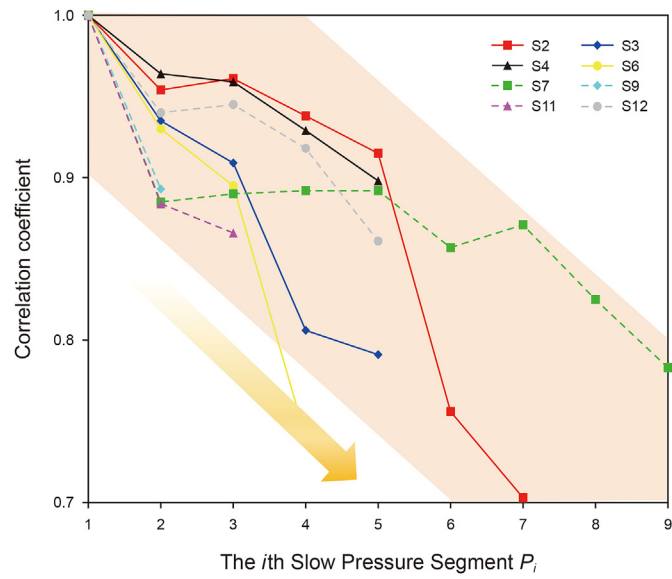**Fig. 20.** The *NESD* of P_1 within all stages.

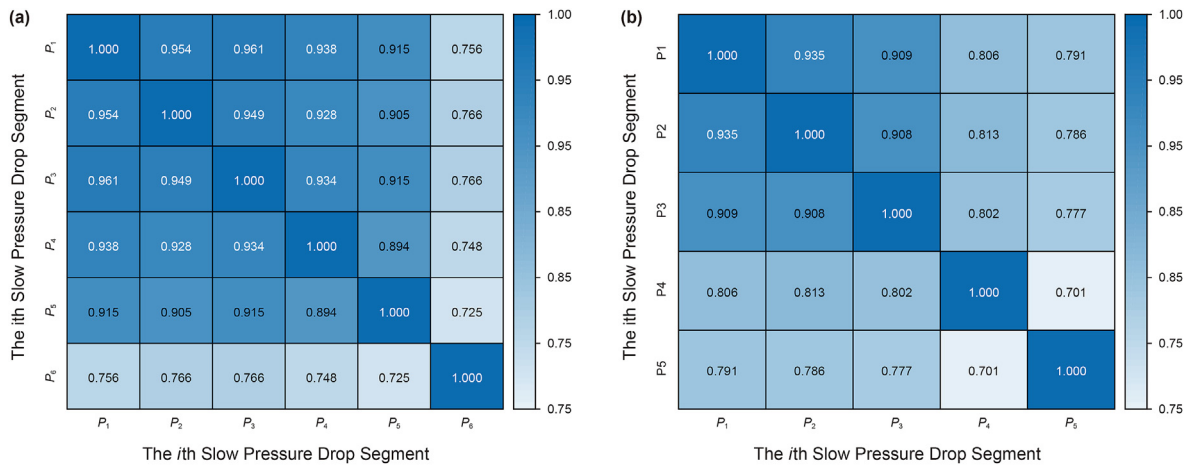**Fig. 22.** The correlation coefficient between P_1 and P_i.

Fig. 21. Heatmap of slow pressure-dropping segment $P_1, P_2, ..., P_n$: (**a**) Stage 2; (**b**) Stage 3.
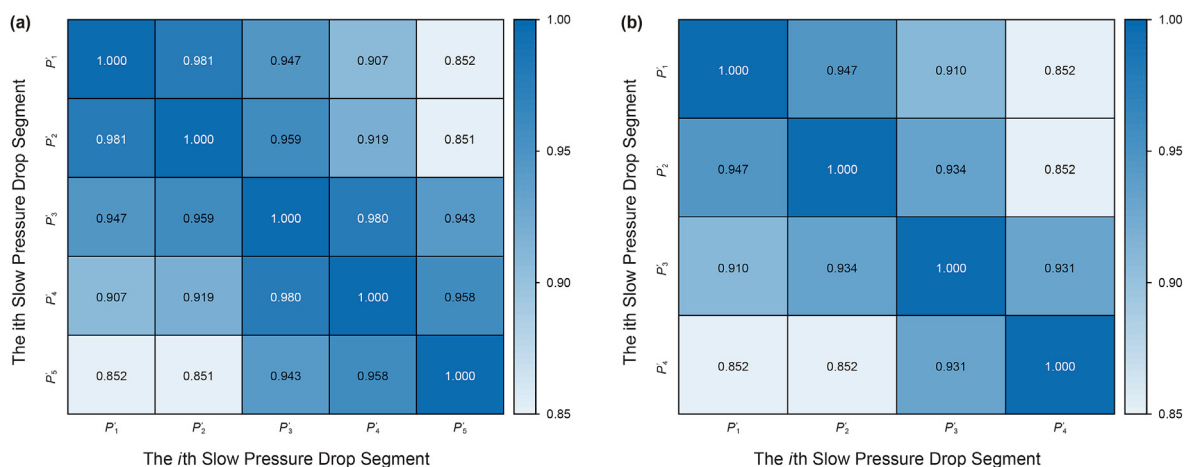
Fig. 23. Heatmap of pressure-dropping segment $P_1', P_2'...P_n'$: (**a**) Stage 2; (**b**) Stage 3.

Declaration of competing interest

The authors declare that they have no known competing financial interests or personal relationships that could have appeared to influence the work reported in this paper.

Acknowledgments

References

Abdrazakov, D., Parkhonyuk, S., Korkin, R., Nikolayev, M., Dyussembayev, D., 2019. Fracturing perspectives in deep HPHT well: comprehensive analysis using high-frequency pressure monitoring, flowback-rebound and step-rate tests. In: SPE Annual Technical Conference and Exhibition, Calgary, Alberta, Canada. https://doi.org/10.2118/196018-MS.

Aliabadi, H.K., Ahmadi, A., Keramat, A., 2020. Frequency response of water hammer with fluid-structure interaction in a viscoelastic pipe. Mech. Syst. Signal Process. 144, 106848. https://doi.org/10.1016/j.ymssp.2020.106848.

Alobaid, H., Khan, A.M., Almulhim, A., Hansen, J., Kabannik, A., 2022a. Comprehensive design and diagnostic approach for horizontal completions in carbonate environment. In: ADIPEC. UAE, Abu Dhabi. https://doi.org/10.2118/210977-MS.

Alobaid, H., Khan, A.M., Hansen, J., Khudorozhkova, A., 2022b. Stimulation efficiency with significantly fewer stages: perforation strategy combined with multimodal diverters and novel nonintrusive monitoring algorithm. In: SPE Annual Technical Conference and Exhibition, Houston, Texas, USA. https://doi.org/10.2118/210472-MS.

Bayle, A., Rein, F., Plouraboué, F., 2023. Frequency varying rheology-based fluid—structure-interactions waves in liquid-filled visco-elastic pipes. J. Sound Vib. 562, 117824. https://doi.org/10.1016/j.jsv.2023.117824.

Bayle, A., Plouraboué, F., 2024. Laplace-domain fluid—structure interaction solutions for water hammer waves in a pipe. J. Hydraul. Eng. 150 (2), 04023062. https://doi.org/10.1061/JHEND8.HYENG-13781.

Bogdan, A.V., Keilers, A., Oussoltsev, D., Lecerf, B., 2016. Real-time interpretation of leak isolation with degradable diverter using high frequency pressure monitoring. In: SPE Asia Pacific Oil & Gas Conference and Exhibition, Perth, Australia. https://doi.org/10.2118/182451-MS.

Borisenko, A., Parkhonyuk, S., Zotov, K., Korkin, R., Kiselev, N.V., Laptev, A., Rapeyko, V.T., 2020. Advanced pressure monitoring technique — new horizons of workover in Russia. In: SPE Russian Petroleum Technology Conference. Virtual. https://doi.org/10.2118/202070-MS.

Carey, M.A., Mondal, S., Sharma, M.M., 2015. Analysis of water hammer signatures for fracture diagnostics. In: SPE Annual Technical Conference and Exhibition, Houston, Texas, USA. https://doi.org/10.2118/174866-MS.

Ciezobka, J., Maity, D., Salehi, I., 2016. Variable pump rate fracturing leads to improved production in the Marcellus Shale. In: SPE Hydraulic Fracturing Technology Conference, The Woodlands, Texas, USA. https://doi.org/10.2118/179107-MS.

Cipolla, C.L., Wright, C.A., 2000. Diagnostic techniques to understand hydraulic fracturing: what? why? and how?. In: SPE/CERI Gas Technology Symposium, Calgary, Alberta, Canada. https://doi.org/10.2118/59735-MS.

Clark, C.J., Miskimins, J.L., Gallegos, D.L., 2018. Diagnostic applications of borehole hydraulic signal processing. SPE/AAPG/SEG Unconventional Resources Technology Conference, Houston, Texas, USA. https://doi.org/10.15530/URTEC-2018-2902141.

Dung, N., Cramer, D., Danielson, T., Snyder, J., Roussel, N., Annie, O., 2021. Practical applications of water hammer analysis from hydraulic fracturing treatments. In: SPE Hydraulic Fracturing Technology Conference and Exhibition. Virtual. https://doi.org/10.2118/204154-MS.

Dunham, E.M., Harris, J.M., Zhang, J., Quan, Y., Mace, K., 2017. Hydraulic fracture conductivity inferred from tube wave reflections. In: SEG Technical Program Expanded Abstracts 2017. Society of Exploration Geophysicists, Houston, Texas, pp. 947—952. https://doi.org/10.1190/segam2017-17664595.1.

Holzhausen, G.R., Gooch, R.P., 1985. Impedance of hydraulic fractures: its measurement and use for estimating fracture closure pressure and dimensions. In: SPE/DOE Low Permeability Gas Reservoirs Symposium. Denver, Colorado. https://doi.org/10.2118/13892-MS.

Hampel, F.R., 1974. The influence curve and its role in robust estimation. J. Am. Stat. Assoc. 69 (346), 383—393. https://doi.org/10.1080/01621459.1974.10482962.

Hu, X.D., Luo, Y.H., Zhou, F.J., Qiu, Y., Li, Z.L., Li, Y.J., 2022. Evaluation of multi-fractures geometry based on water hammer signals: a new comprehensive model and field application. J. Hydrol. 612 (B), 128240. https://doi.org/10.1016/j.jhydrol.2022.128240.

Hwang, J., Szabian, M.J., Sharma, M., 2017. Hydraulic fracture diagnostics and stress interference analysis by water hammer signatures in multi-stage pumping data. SPE/AAPG/SEG Unconventional Resources Technology Conference, Austin, Texas, USA. https://doi.org/10.15530/URTEC-2017-2687423.

Iriarte, J., Merritt, J., Kreyche, B., 2017. Using water hammer characteristics as a fracture treatment diagnostic. SPE Oklahoma City Oil and Gas Symposium, Oklahoma City, Oklahoma, USA. https://doi.org/10.2118/185087-MS.

Kabannik, A., Parkhonyuk, S., Korkin, R., Litvinets, F., Dunaeva, A., Nikolaev, M., Usoltsev, D., 2018. Can we trust the diversion pressure as a decision-making tool: novel technique reveals the truth. Abu Dhabi International Petroleum Exhibition & Conference, Abu Dhabi, UAE. https://doi.org/10.2118/193180-MS.

Korkin, R., Parkhonyuk, S., Fedorov, A., Badazhkov, D., Kabannik, A., 2020. High frequency pressure monitoring and data analytics for stimulation efficiency determination: new perspectives or potential limits. SPE Hydraulic Fracturing Technology Conference and Exhibition, The Woodlands, Texas, USA. https://doi.org/10.2118/199762-MS.

Liang, C., O'Reilly, O., Dunham, E.M., Moos, D., 2017. Hydraulic fracture diagnostics from Krauklis-wave resonance and tube-wave reflections. Geophysics 82 (3), D171—D186. https://doi.org/10.1190/geo2016-0480.1.

Luo, Y.H., Hu, X.D., Zhou, F.J., Qiu, Y., Lu, X.T., Li, J.Y., Wang, Y.J., 2023. A new water hammer decay model: analyzing the interference of multiple fractures and perforations on decay rate. SPE J. 28, 1973—1985. https://doi.org/10.2118/214658-PA.

Ma, X., Zhou, F.P., Ortega Andrade, J.A., Gosavi, S., Burch, D., 2019. Evaluation of water hammer analysis as diagnostic tool for hydraulic fracturing. SPE/AAPG/SEG Unconventional Resources Technology Conference, Denver, Colorado, USA. https://doi.org/10.15530/urtec-2019-935.

Mahmoud, A., Gowida, A., Aljawad, M., Al Ramadan, M., Ibrahim, A., 2021. Advancement of hydraulic fracture diagnostics in unconventional formations. Geofluids, 4223858. https://doi.org/10.1155/2021/4223858.

Ng, A., Jordan, M.I., 2002. On discriminative vs. generative classifiers: a comparison of logistic regression and naive Bayes. Adv. Neural Inf. Process. Syst. 14 (2), 841—848. https://api.semanticscholar.org/CorpusID:296750.

Oppenheim, A.V., Willsky, S., Young, A.T., 1983. Signals and Systems. Prentice-Hall.

Ott, R.L., Longnecker, M., 2016. An Introduction to Statistical Methods and Data

Analysis, seventh ed. Brooks/Cole, Cengage Learning, Belmont, CA.

Panjaitan, M.L., Moriyama, A., McMillan, D., Dunaeva, A., Rutledge, L., Xu, J., Parkhonyuk, S., Kabannik, A., Korkin, R., Warren, M., Shanmugam, V., 2018. Qualifying diversion in multi-cluster horizontal well hydraulic fracturing in Haynesville Shale using water hammer analysis, step-down test and microseismic data. SPE Hydraulic Fracturing Technology Conference and Exhibition, the Woodlands, Texas, USA. https://doi.org/10.2118/189850-MS.

Parkhonyuk, S., Fedorov, A., Kabannik, A., Korkin, R., Nikolaev, M., Tsygulev, I., 2018a. Measurements while fracturing: nonintrusive method of hydraulic fracturing monitoring. SPE Hydraulic Fracturing Technology Conference and Exhibition, The Woodlands, Texas, USA. https://doi.org/10.2118/189886-MS.

Parkhonyuk, S., Korkin, R., Kabannik, A., Fedorov, A., Nikolaev, M., Litvinets, F., 2018b. Novel monitoring technology helps to make informed decisions and maximize the efficiency of completion strategy. In: SPE/AAPG/SEG Unconventional Resources Technology Conference, Houston, Texas, USA. https://doi.org/10.15530/URTEC-2018-2885828.

Pearson, K., 1896. Mathematical Contributions to the Theory of Evolution. Dulau and Co, London.

Qiu, Y., Hu, X.D., Zhou, F.J., Li, Z.L., Li, Y.J., Luo, Y.H., 2022. Water hammer response characteristics of wellbore-fracture system: multi-dimensional analysis in time, frequency and quefrency domain. J. Pet. Sci. Eng. 213, 110425. https://doi.org/10.1016/j.petrol.2022.110425.

Rodionov, Y., Defeu, C., Gakhar, K., Mullen, K., Mayo, J.T., Shan, D., Usoltsev, D., Ejofodomi, E., 2017. Optimization of infill well development using a novel farfield diversion technique in the Eagle Ford Shale. SPE/AAPG/SEG Unconventional Resources Technology Conference, Austin, Texas, USA. https://doi.org/10.15530/URTEC-2017-2670497.

Urbanowicz, K., Bergant, A., Stosiak, M., Karpenko, M., Bogdevičius, M., 2023. Developments in analytical wall shear stress modelling for water hammer phenomena. J. Sound Vib. 562, 117848. https://doi.org/10.1016/j.jsv.2023.117848.

Urbanowicz, K., Jing, H.X., Bergant, A., Stosiak, M., Lubecki, M., 2021. Progress in Analytical Modeling of Water Hammer. Volume 1: Aerospace Engineering Division Joint Track. Computational Fluid Dynamics. https://api.semanticscholar.org/CorpusID:244200072.

Wang, X.L., Hovem, K., Moos, D., Quan, Y.L., 2008. Water hammer effects on water Injection well performance and longevity. SPE International Symposium and Exhibition on Formation Damage Control, Lafayette, Louisiana, USA. https://doi.org/10.2118/112282-MS.

Zeng, B., Zhou, N.Y., Guo, X.W., Wang, Y.T., Fu, Y.L., Wang, G., Korkin, R., Fedorov, A., Borisenko, A., Luo, Y., Li, H.Y., Zhang, J., 2023. New high-frequency pressure monitor algorithm guided multistage stimulation for long lateral without mechanical isolation. SPE Annual Technical Conference and Exhibition, San Antonio, Texas, USA. https://doi.org/10.2118/214867-MS.